Int J Adv Manuf Technol (2016) 84:2499–2514
DOI 10.1007/s00170-015-7851-2

ORIGINAL ARTICLE

A novel approach to determination of wheel position and orientation for five-axis CNC flute grinding of end mills

Liming Wang [1,2] · **Zezhong Chevy Chen** [3] · **Jianfeng Li** [1,2] · **Jie Sun** [1,2]

Received: 25 March 2015 / Accepted: 13 September 2015 / Published online: 3 October 2015

Abstract In practice, the flutes of end mills are ground using CNC grinding machines via controlling the grinding wheel's position and orientation to guarantee the designed flute parameters including rake angle, flute angle, helix angle, and core radius. However, for the previous researches, the designed flute profile was ground via building a specific grinding wheel with a free-form profile using two-axis CNC grinder. And, the free-form grinding wheel will greatly increase the manufacturing cost, which is too complicated to implement in practice. In this research, the flute-grinding processes were developed with a standard grinding wheel via five-axis CNC grinding operations. The mathematical representation of machined flute parameters was deduced in terms of the grinding wheel's position and orientation. The geometrical constraints to avoid interference and abnormal flute profile for the five-axis CNC fluting were first developed in this work. Finally, the difference between the designed flute parameters and the machined flute parameters were formulated as a constrained optimization problem so as to determine the wheel's position and orientation. The set of effective initial points for this optimization model was found mainly distributed the first quadrant of the contact area. The *fminsearch* function in Matlab toolbox was recommended to solve the optimization model due to its capability of handling discontinuity problem. The solution obtained in optimization model and the corresponding machined flute parameter were verified and compared with Boolean simulation in CATIA to confirm the validity and efficiency of the proposed approach. The results showed that the accuracy of machined flute parameters could achieve 1e-3 mm and 1e-2°, which satisfied the machining tolerance. This study provides a general solution for the CNC fluting operations and could be extended to grind complex surface of end mills in the future study.

Keywords End mill · Flute grinding · Five-axis CNC grinding · Grinding wheel

✉ Liming Wang
liming_wang@sdu.edu.cn

[1] School of Mechanical Engineering, Shandong University, Jinan, China

[2] Key Laboratory of High Efficiency and Clean Mechanical Manufacture, Ministry of Education, Shandong University, Jinan, China

[3] Department of Mechanical and Industrial Engineering, Concordia University, Montreal, Quebec, Canada

1 Introduction

Flutes make up the main part of the solid end mill, which can significantly affect the tool's life and machining quality in milling processes. In practice, the flute is machined by the grinding wheel moving with a helix motion using CNC grinding machines [1, 2]. Figure 1a shows a general setting of grinding end mills. The grinding wheel is mounted above the tool bar with a specific position and orientation relative to the grinding wheel in the machine coordinate system. With the intersection between the grinding wheel and the tool bar, the flute profile of end mills is formed and the flute parameters are also guaranteed through setting the grinding wheel with a specific position and orientation in the grinding processes. The generated flute profile is described by three flute parameters: rake angel γ, core diameter r_c, and flute angle ϕ shown in Fig. 1b.

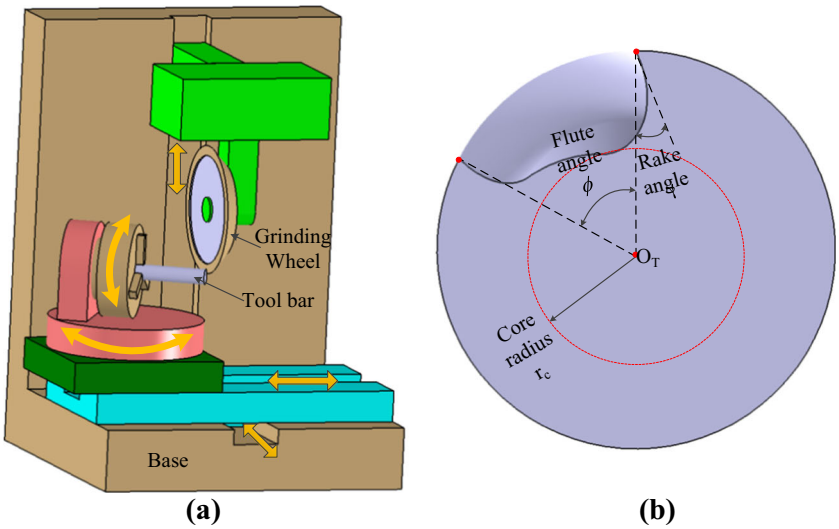

Fig. 1 Illustration of flute-grinding processes: **a** CNC grinding machine and **b** generated flute profile and flute parameters

Geometrically, the flute profile is determined by two issues: (1) the grinding wheel profile and (2) the grinding operations. To establish the geometrical relation between the profile of grinding wheel and flute shape, Kaldor [3] first defined two basic geometric problems in the flute-grinding processes, that is, the direct problem and the inverse problem. The direct problem refers to modeling the generated flute profile for a given grinding wheel, while the inverse problem is to determine the wheel profile for a designed flute profile. Ehmann et al. [4] calculated the contact line between the grinding wheel and tool bar using conjugate theory, that is, the common normal at the contact point between the wheel surface and flute surface should intersect with the central axis of the tool bar. Based on the conjugate theory, the general analytical representation of the generated flute profile and determination of wheel profile were discussed by the following researchers [5–9]. However, the methods introduced above with conjugate theory can only be available while the wheel surface is C^1 continual. However, in practical, the wheel surface is C^0 continual at the wheel edge point. It was found that the flute profile was partly generated by the envelope of the wheel profiles and partly by sweeping the wheel edge, which would result in interference or abnormal profile of flutes in the five-axis CNC grinding processes. For this case, the contact line method cannot be used to predict the machined flutes. Boolean operation [10–12] would be a solution to cope with this problem, but more iteration steps are required to achieve a high accuracy.

Besides, the basic idea for inverse problem is to grind the designed flute profile by dressing the grinding wheel with a specific profile (free-form) and also configured the wheel with a fixed position and orientation [13–15]. There are only two motions that can be controlled in the grinding processes, that is, translation and rotation about the tool axis. Due to the limitation of two-axis configuration, the grinding wheel is required predressed with specific profile [16–18] and the dressed grinding wheel can only be used for the specific flute shape, which will increase the cost of manufacturing end mill. Actually, in engineering, the grinding wheel is generally standardized [19], which means that the shape of grinding wheel is fixed before grinding and the designed flute parameters are guaranteed with controlling the grinding operations. Until now, to the author's knowledge, there have been very few literatures on modeling the flute parameters through controlling the wheel's position and orientation. Hereto, in this research, a five-axis CNC grinding algorithm was proposed to grind the designed flute parameters precisely with standard grinding wheel. The flute profile and corresponding parameters were directly deduced in the cross section using the envelope theory. The geometrical constraints were first developed in this work to avoid interference and abnormal flute profile for the five-axis CNC fluting. Determination of the wheel position and orientation for the designed flute parameters were converted to a constrained optimization problem based on the kinematics of five-axis CNC flute-grinding model, and it finally proved to be solved efficiently and precisely with several examples.

For the following sections, this paper was organized as follows. Section 2 developed the kinematics of five-axis flute-grinding processes and expressed the generated flute parameters from the flute profile. Section 3 discussed the effect of wheel's position and orientation on the flute profile in the grinding processes so as to find the condition to avoid interference and abnormal profile of flutes. In Sect. 4, an optimization model was proposed to determine the wheel position and orientation for the designed flute parameters. Conclusions were given in Sect. 5.

2 Flute profile modeling with five-axis CNC grinding

2.1 Grinding wheel modeling

The helix flute is generated with intersection between the grinding wheel and the cutter with a helix motion. The working area of grinding wheel occurs at the wheel edge and wheel surface shown in Fig. 2. A standard cylindrical grinding wheel is applied in this research, which consists of two functional parts: the peripheral surface and the wheel edge. The wheel model is governed by the parameters wheel radius R and wheel width H. A wheel coordinate system noted as $\boldsymbol{O_g}$ is fixed at the center of wheel edge. As described in Fig. 2, $\boldsymbol{Z_g}$ axis is pointing from the left plane to the end plane, $\boldsymbol{Y_g}$ axis is in the vertical direction, and $\boldsymbol{X_g}$ axis is horizontal. A parameterized representation of the grinding wheel referencing to $\boldsymbol{O_g}$ is deduced regarding to the variable h and θ in Eq. (1). The wheel edge can be represented by setting $h=0$, that is $W_g(0,\theta)$.

$$W_g(h,\theta) = \begin{bmatrix} R\cdot\cos\theta \\ R\cdot\sin\theta \\ h \end{bmatrix}, \tag{1}$$

where R is the wheel radius, h and θ are the wheel parametric variables with $h\in[0,\mathrm{H}]$ and $\theta\in[0,2\pi]$.

2.2 Five-axis flute-grinding processes

In order to describe the flute-grinding processes, a tool coordinate system noted as $\boldsymbol{O_T}$ is established and illustrated in Fig. 3, of which the origin $\boldsymbol{O_T}$ is located at the center of left end of the tool bar. As described in Fig. 3, $\boldsymbol{Z_T}$ axis is the tool axis pointing from the left to the end plane, $\boldsymbol{Y_T}$ axis is in the vertical direction, and $\boldsymbol{X_T}$ axis is horizontal.

The five-axis flute-grinding processes can be implemented with two operations: (1) machine configuration (also called wheel setting) and (2) the relative helix motion between the tool

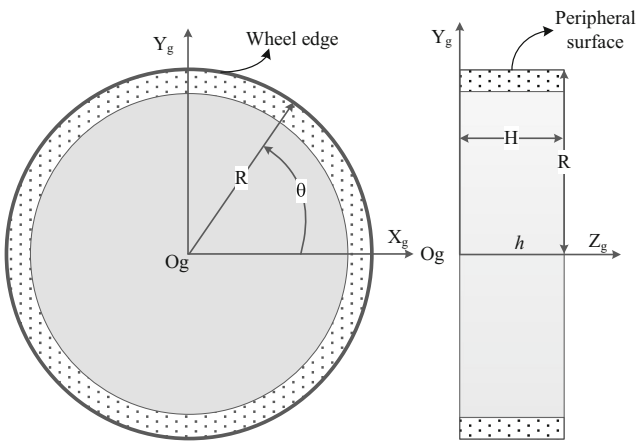

Fig. 2 Illustration of the cylindrical grinding wheel

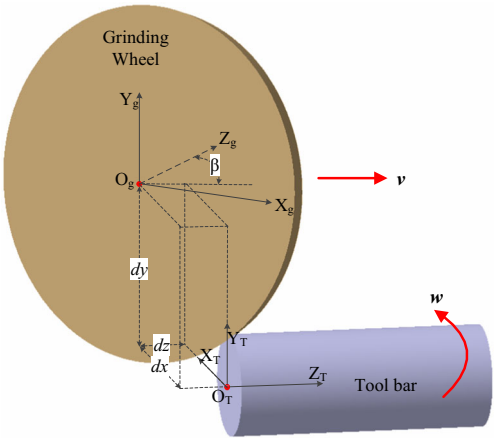

Fig. 3 Five-axis CNC flute-grinding processes

bar and grinding wheel. Initially, the grinding wheel is configured with a specified position and orientation represented by the wheel center coordinated value $[\,dx \quad dy \quad dz\,]$ and setup angle β shown in Fig. 3. The configuration processes can be resolved into several motions reference to $\boldsymbol{O_T}$: rotating about Yaxis by β; translation along X, Y, and Z axis by dx, dy, and dz, respectively. The configuration operation is expressed in $\boldsymbol{O_T}$ using the homogeneous coordinate transformation in Eq. (2). The translation in Z axis will not affect the final flute profile and flute parameters; therefore, dx, dy, and β (three parameters) are wheel position and orientation parameters which are required to be determined in the flute-grinding processes. For simplification, in the following calculation, dz is set as zero.

$$\begin{aligned}\mathbf{M_1} &= trans(\mathrm{Z_T}, dz)\cdot trans(\mathrm{Y_T}, dy)\cdot trans(\mathrm{X_T}, dx)\cdot rot(\mathrm{Y_T}, \beta)\\ &= \begin{bmatrix} \cos\beta & 0 & \sin\beta & dx \\ 0 & 1 & 0 & dy \\ -\sin\beta & 0 & \cos\beta & dz \\ 0 & 0 & 0 & 1 \end{bmatrix}\end{aligned} \tag{2}$$

After machine configuration, the grinding wheel moves along Z_T axis with a translation velocity v, while the cutter rotate with a specific angular velocity ω to generate the helix flute surface shown in Fig. 3. This operation can be represented in the tool coordinate system using another homogeneous matrix in Eq. (3):

$$\begin{aligned}\mathbf{M_2} &= rot(z,\omega\cdot t)\cdot trans(z, v\cdot t)\\ &= \begin{bmatrix} \cos(\omega\cdot t) & -\sin(\omega\cdot t) & 0 & 0 \\ \sin(\omega\cdot t) & \cos(\omega\cdot t) & 0 & 0 \\ 0 & 0 & 1 & 0 \\ 0 & 0 & 0 & 1 \end{bmatrix}\cdot\begin{bmatrix} 1 & 0 & 0 & 0 \\ 0 & 1 & 0 & 0 \\ 0 & 0 & 1 & v\cdot t \\ 0 & 0 & 0 & 1 \end{bmatrix}\\ &= \begin{bmatrix} \cos(\omega\cdot t) & -\sin(\omega\cdot t) & 0 & 0 \\ \sin(\omega\cdot t) & \cos(\omega\cdot t) & 0 & 0 \\ 0 & 0 & v\cdot t & 0 \\ 0 & 0 & 0 & 1 \end{bmatrix}\end{aligned} \tag{3}$$

Integrating Eqs. (1), (2), and (3), the representation of grinding wheel in the five-axis flute-grinding processes at any instant is obtained in the tool coordinate system shown in Eq. (4):

$$\begin{bmatrix} \mathbf{W}_{\mathrm{T}}(h,\theta,t) \\ 1 \end{bmatrix} = \mathbf{M}_2 \cdot \mathbf{M}_1 \cdot W_{\mathrm{g}} = \begin{bmatrix} dx \cdot \cos(\omega t) - dy \cdot \sin(\omega t) + h \cdot \sin\beta \cdot \cos(\omega t) - R \cdot \sin\theta \cdot \sin(\omega t) + R \cdot \cos\beta \cos\theta \cdot \cos(\omega t) \\ dx \cdot \sin(\omega t) + dy \cdot \cos(\omega t) + h \cdot \sin\beta \cdot \sin(\omega t) + R \cdot \sin\theta \cdot \cos(\omega t) + R \cdot \cos\beta \cdot \cos\theta \cdot \sin(\omega t) \\ h \cdot \cos\beta + \mathrm{v}t - R \cdot \sin\beta \cdot \cos\theta \\ 1 \end{bmatrix} \tag{4}$$

And also, the rotation velocity and translation velocity are governed by the helix angle λ using the following equation:

$$\tan\lambda = \frac{r_{\mathrm{T}} \cdot \omega}{v} \tag{5}$$

where r_{T} is the tool radius and λ is the helix angle.

As aforementioned, geometrically, the flute is generated between intersection of the grinding wheel and cutter in 3D space. For previous researches [2, 5], the intersection is expressed as the contact line deduced with the conjugate theory. And then, the 3D flute surface is obtained through sweeping the contact curve with a helix motion. However, in this research, the Eq. (4) is first truncated within the cross section to obtain the flute profile by setting Z element as a constant shown in Eq. (6).

$$h \cdot \cos\beta + vt - R \cdot \sin\beta \cdot \cos\theta + dz = \mathrm{C} \tag{6}$$

where $\mathrm{C} \in [0, \mathrm{L}]$ and L is the flute length along the $\boldsymbol{Z}_{\mathbf{T}}$ direction.

Solving Eq. (6), get the expression $t^* = \frac{R \cdot \sin\beta \cdot \cos\theta + \mathrm{C} - h \cdot \cos\beta - dz}{v}$.

And, the flute profile generated by the intersection grinding wheel within tool's cross section is expressed in terms of t^* in Eq. (7).

$$F_{\mathrm{T}}(h,\theta) = \begin{bmatrix} dx \cdot \cos t - dy \cdot \sin t^* + h \cdot \sin\beta \cdot \cos t^* - R \cdot \sin\theta \cdot \sin t^* + R \cdot \cos\beta \cdot \cos\theta \cdot \cos t^* \\ dx \cdot \sin t + dy \cdot \cos t^* + h \cdot \sin\beta \cdot \sin t^* + R \cdot \sin\theta \cdot \cos t^* + R \cdot \cos\beta \cdot \cos\theta \cdot \sin t^* \end{bmatrix} \tag{7}$$

As shown in Fig. 4, the flute profile denoted by F_{T} is generated by a family of curves, which can be regarded as discretizing the grinding wheel into a group of disks and each disk is swept and intersected with the cross section. Consequently, the flute profile in the cross section is enveloped by the family curves. The result flute profile consists of two parts: (1) the curve generated by swept wheel edge and (2) the curve generated by envelope curves. The first part can be calculated through setting $h=0$ in Eq. (8).

$$F_{\mathrm{T}}(0,\theta) = \begin{bmatrix} dx \cdot \cos t^* - dy \cdot \sin t^* - R \cdot \sin\theta \cdot \sin t^* + R \cdot \cos\beta \cdot \cos\theta \cdot \cos t^* \\ dx \cdot \sin t^* + dy \cdot \cos t^* + R \cdot \sin\theta \cdot \cos t^* + R \cdot \cos\beta \cdot \cos\theta \cdot \sin t^* \end{bmatrix} \tag{8}$$

According to the envelope theory, the enveloped part of flute profile is obtained by Eq. (7) with the condition in Eq. (9). Equation (9) is solved easily via numerical methods (golden search method) and verified in Fig. 4 with the envelope points which located in the envelope curve.

$$\begin{vmatrix} \frac{\partial x}{\partial \theta} & \frac{\partial y}{\partial \theta} \\ \frac{\partial x}{\partial h} & \frac{\partial y}{\partial h} \end{vmatrix} = 0. \tag{9}$$

Mathematically, we can represent the relationship between θ^* and $h$for the envelope points with a general solution denoted as $\theta^* = f_{envelope}(h)$.

2.3 Flute parameters formulation within the cross section

Generally, the flute parameters including rake angle, core radius, and flute angle are defined within the cross section. As shown in Fig. 4, the flute profile is described in the reference of the tool coordinate system O_{T}. In order to define the flute parameters, two key points is illustrated as the following: The start point P_{S} and end point P_{E} are the intersection of flute profile with the tool boundary (tool circle), which are located in the flute profile curve with the geometric relation $|O_{\mathrm{T}}P_{\mathrm{S}}| = |O_{\mathrm{T}}P_{\mathrm{E}}| = r_{\mathrm{T}}$. Here, the point P_{S} and point P_{E} can be

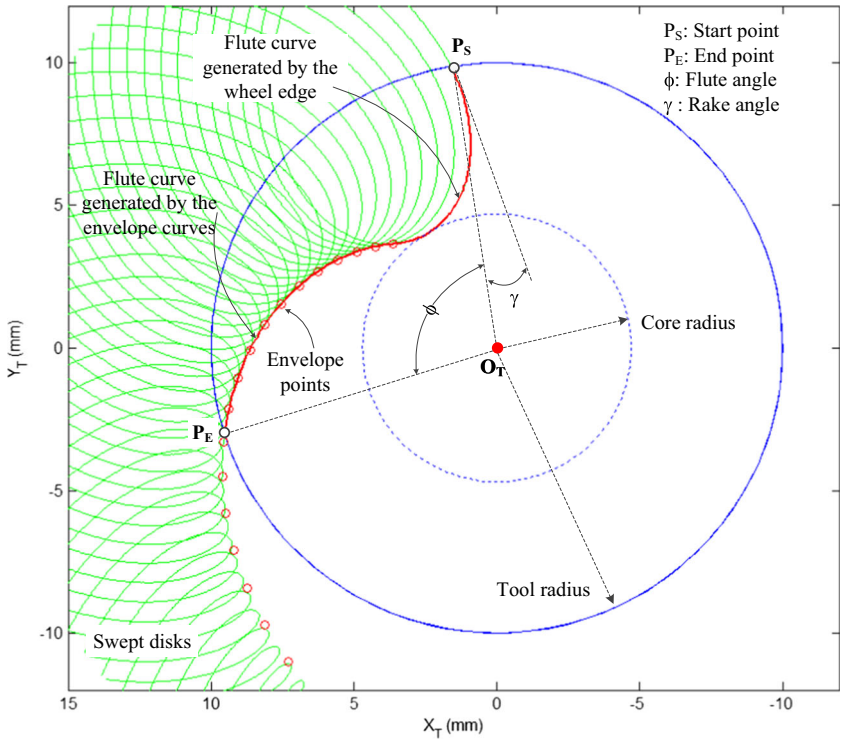

Fig. 4 Flute profile generated by envelope grinding wheel

expressed by recalling Eqs. (7) and (8) using the following equation:

$$P_S(0,\theta_S^*) = \begin{bmatrix} dx\cdot\cos t^* - dy\cdot\sin t^* - R\cdot\sin\theta_S^*\cdot\sin t^* + R\cdot\cos\beta\cdot\cos\theta_S^*\cdot\cos t^* \\ dx\cdot\sin t^* + dy\cdot\cos t^* + R\cdot\sin\theta_S^*\cdot\cos t^* + R\cdot\cos\beta\cdot\cos\theta_S^*\cdot\sin t^* \end{bmatrix}. \quad (10)$$

And, θ_S^* satisfy the following condition:

$$R^2 + dx^2 + dy^2 + 2R\cdot dy\cdot\sin\theta_S^* + 2R\cdot dx\cdot\cos\beta\cdot\cos\theta_S^* - R^2\cdot\sin^2\beta\cdot\cos^2\theta_S^* = r_T^2 \quad (11)$$

The solution for θ_S^* will be introduced in the following section.

$$P_E(\theta_E^* \quad h_E^*) = \begin{bmatrix} dx\cdot\cos t^* - dy\cdot\sin t^* + h_E^*\cdot\sin\beta\cdot\cos t^* - R\cdot\sin\theta_E^*\cdot\sin t^* + R\cdot\cos\beta\cdot\cos\theta_E^*\cdot\cos t^* \\ dx\cdot\sin t^* + dy\cdot\cos t^* + h_E^*\cdot\sin\beta\cdot\sin t^* + R\cdot\sin\theta_E^*\cdot\cos t^* + R\cdot\cos\beta\cdot\cos\theta_E^*\cdot\sin t^* \end{bmatrix} \quad (12)$$

Similarly, θ_E^* is governed by the following equation:

$$\begin{cases} R^2 + dx^2 + dy^2 + 2R\cdot dy\cdot\sin\theta_E^* + 2\mathrm{R}\cdot dx\cdot\cos\beta\cdot\cos\theta_E^* + h_E^{*2}\cdot\sin^2\beta - R^2\cdot\sin^2\beta\cdot\cos^2\theta_E^* = r_T^2 \\ \theta_E^* = f_{envelope}(h_E^*) \end{cases}, \quad (13)$$

where $h_E^* \in [0 \quad H]$. And also, golden search method was used to solve Eqs. (11) and (13) within the search range: $\theta_s^* \in [0 \quad 2\pi]$ and $h_E^* \in [0 \quad H]$.

Since the two points P_S and P_E were deduced with the above equations, the flute angle ϕ refers to the open angle $\angle P_S O_T P_E$ between the start point P_S and end point P_E, which can be expressed using the vector form in Eq. (14).

$$\phi = a\cos\left(\frac{O_T P_S \cdot O_T P_E}{|O_T P_S| \cdot |O_T P_E|}\right) \quad (14)$$

The core radius r_c is the minimum distance from the flute curve to origin $\boldsymbol{O_T}$, which can be calculated using the following expression in Eq. (15).

$$r_c = min\left(sqrt\left(x^2 + y^2\right)\right),\ \text{where}[x, y] \in F_T. \tag{15}$$

Besides, the rake angle γ is also calculated as the angle between the tangent TP_S shown in Eq. (16) and radius direction P_EO_T at point P_S.

$$TP_S = \frac{dF_s\left(0, \theta_S^*\right)}{d\theta} = \begin{bmatrix} -dx\cdot\sin t^*\cdot\frac{dt^*}{d\theta}\left(\theta_S^*\right) - dy\cdot\cos t^*\cdot\frac{dt^*}{d\theta}\left(\theta_S^*\right) - R\cdot\cos\theta_S^*\cdot\sin t^* - R\cdot\sin\theta_S^*\cdot\cos t^*\cdot\frac{dt^*}{d\theta}\left(\theta_S^*\right) \\ -R\cdot\cos\beta\cdot\sin\theta_S^*\cdot\cos t^* - R\cdot\cos\beta\cdot\cos\theta_S^*\cdot\sin t^*\cdot\frac{dt^*}{d\theta}\left(\theta_S^*\right) \\ dx\cdot\cos t^*\cdot\frac{dt^*}{d\theta}\left(\theta_S^*\right) - dy\cdot\sin t^*\cdot\frac{dt^*}{d\theta}\left(\theta_S^*\right) + R\cdot\cos\theta_S^*\cdot\cos t^* - R\cdot\cos\theta_S^*\cdot\sin t^*\cdot\frac{dt^*}{d\theta}\left(\theta_S^*\right) \\ -R\cdot\cos\beta\cdot\sin\theta_S^*\cdot\sin t^* + R\cdot\cos\beta\cdot\cos\theta_S^*\cdot\cos t^*\cdot\frac{dt^*}{d\theta}\left(\theta_S^*\right) \end{bmatrix} \tag{16}$$

where $\frac{dt^*}{d\theta} = -\frac{R\cdot\sin\beta\cdot\sin\theta}{v}$.

Hereto, the expression of rake angle γ is obtained with the vector angle with the following expression Eq. (17):

$$\gamma = a\cos\left(\frac{TP_S\cdot P_EO_T}{|TP_S|\cdot|P_EO_T|}\right) \tag{17}$$

With the above deduction, the flute parameters are related with the grinding wheel shape, wheel positions, and orientation. As mentioned, in practice, the grinding wheel is scandalized with a fixed shape, which means that the grinding wheel parameters are constant. Therefore, in this research, for a given cylindrical grinding wheel, the flute parameters are expressed in a general function in terms of wheel position $[dx \quad dy]$ and orientation β in Eq. (18):

$$\begin{cases} \gamma = f_{rake}(dx \quad dy \quad \beta) \\ \phi = f_{flute}(dx \quad dy \quad \beta) \\ r_c = f_{core}(dx \quad dy \quad \beta) \end{cases} \tag{18}$$

where r_c, ϕ, and γ represent the flute parameters core radius, flute angle, and rake angle, respectively.

3 Investigation of wheel's position and orientation on flute profile

Based on the above flute-grinding model with envelope theory, the flute profile is closely related with the setting of grinding wheel's position and orientation. With different combination setting parameters, there will be various flute shapes generated. A proper initial wheel setting parameters are required to guarantee the flute shape. Otherwise, interference or abnormal flute profile will happen as shown in the following figures. In this section, the geometrical relation between the grinding wheel and the cutter is investigated considering the engineering practice based on proposed envelope flute profile within the cross section to avoid the flute interference and abnormal flute profile.

3.1 Contact area for the grinding wheel and cutter

Physically, the flute is machined by intersection between grinding wheel and cutter. Therefore, in the flute-grinding processes, the grinding wheel should always contact with the cutter in space. Besides, in order to avoid overcut of core radius, the intersection part should not exceed the boundary of core radius. This condition can be modeled through projecting the profiles of cutter and grinding wheel edge in the cross section (X_TY_T plane) shown in Fig. 5.

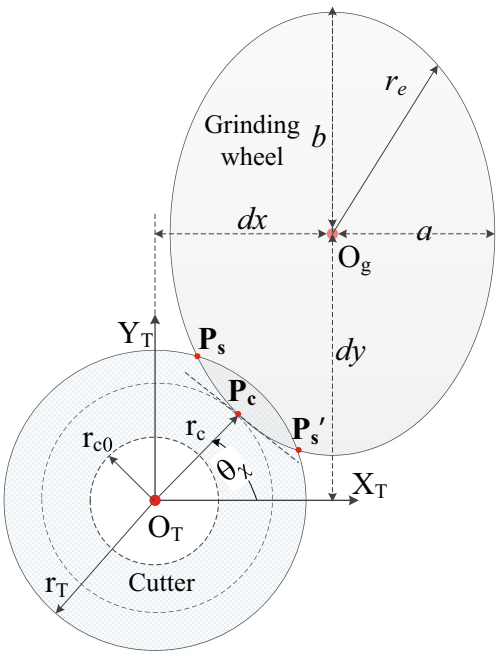

Fig. 5 Projection of cutter profile and wheel edge within cross section

In Fig. 5, the cutter profile is simplified by a circle with a tool radius r_T and core radiusr_c. And, $\boldsymbol{O_g}$ is the center of ellipse with the wheel location $[dx \quad dy]$ in the tool coordinate system. The ellipse of grinding wheel projection can be determined by wheel's position and orientation expressed in Eq. (19):

$$r_e = \begin{bmatrix} dx + a \cdot \cos\theta_e \\ dy + b \cdot \sin\theta_e \end{bmatrix}, \tag{19}$$

where a and b are the radius on the x and y axes respectively, and θ_e is the parameter range $\theta_e \in [0, 2\pi]$. $a = R \cdot \cos\beta$ and $b = R$.

In addition, the contact point $\boldsymbol{P_c}$ (see Fig. 5) with coordinate value $[x_c \quad y_c]$ is the minimum distance from the wheel ellipse to point $\boldsymbol{O_T}$. In order to keep that the wheel ellipse is intersecting with the cutter circle while not exceeding the core circle, the point $\boldsymbol{P_c}$ should be located inside of annulus area which is bounded between the core and tool radius denoted by a set $\boldsymbol{S}$ in Eq. (20).

$$S = \left\{ r_c(\theta_c) \middle| r_{c0} \le r_c \le r_T \right\} \tag{20}$$

The area $\boldsymbol{S}$ is feasible set for wheel and cutter to guarantee intersection with each other. As shown in Fig. 5, the ellipse is tangent with a specific circle at the contact point $\boldsymbol{P_c}$. The geometrical equation between contact point $\boldsymbol{P_c}$ and $\boldsymbol{O_g}$ is deduced as the following:

$$r_c \cdot r_e' = 0 \tag{21}$$

where r_c is the vector $\boldsymbol{O_T P_c}$, r_e' is the derivative of r_e expressed in Eq. (21) at point $\boldsymbol{P_c}$.

Solving Eq. (21), we get the expression $\theta_e^* = \arctan(b \cdot y_c, a \cdot x_c)$, where $r_c = \begin{bmatrix} x_c \\ y_c \end{bmatrix}$ and $[x_c \quad y_c] \in S$.

Substituting θ_e^* into Eq. (19), the expression of wheel position $\boldsymbol{O_g}$ in terms of the contact point $\boldsymbol{P_c}$ referring to tool coordinate system is obtained in Eq. (22):

$$O_g = \begin{bmatrix} x_c - a \cdot \cos\theta_e^* \\ y_c - b \cdot \sin\theta_e^* \end{bmatrix} \tag{22}$$

Through the above geometrical relation between wheel location $\boldsymbol{O_g}$ and contact point $\boldsymbol{P_c}$, the intersection area $\boldsymbol{S}$ can be mapping to a feasible set as the constraint of the wheel setting parameters. In practice, the cutter and grinding wheel are only contact in the upper area of $\boldsymbol{S}$, that is $\theta_c \in [0 \quad \pi]$. Therefore, in this research, various initial wheel position points in the upper area of $\boldsymbol{S}$ are investigated to test the flute shape.

3.2 Interference of flute profile

In the flute-grinding processes, the wheel trajectory is typically defined with a helix motion related with the helix angle and wheel configuration parameters. Improper wheel position and orientation in the grinding processes would result in the interference between the grinding wheel and machined flute surface. In practice, interference generally happened in the rake face of flute, which is ground by the wheel edge. As shown in Fig. 6, an example is given to demonstrate the interference of flute-grinding processes. The cylindrical grinding wheel with parameters width 20 mm and radius 75 mm is employed in this case. The wheel position and orientation parameter are described as the following: dx=8.766, dy=79.426, and β=60.00, and the cutter is modeled with a radius 10 mm and helix angle 45°. The machined flute is shown in the following figure. The dotted line in the cross section is the rake face of designed flute profile, and the solid line is the machined flute profile. It is observed that interference happened on the rake face of designed flute. The rake face profile is destroyed by the succeeding grinding of wheel edge in the grinding processes, which generally caused by a larger setup angle. In practice, the value of wheel setup angle is a recommended setting around the helix angle λ to avoid interference.

In this section, in order to avoid the interference, for a given wheel position, a limit range for wheel orientation β was investigated through modeling the rake face profile generated by the wheel edge grinding. Recalling the flute envelope modeling in above section, a group of flute profiles are generated and plotted in Fig. 7. It is observed that the interference happened in the last two plots with wheel setup angle: 56° and 60°, which is coinciding with the fact that the larger setup angle tends to result in interference.

As shown in Fig. 8, the red twist curve shows the envelope curve generated by the wheel edge. Point P_S and P_S' in the figure are the intersections between the twist curve and the

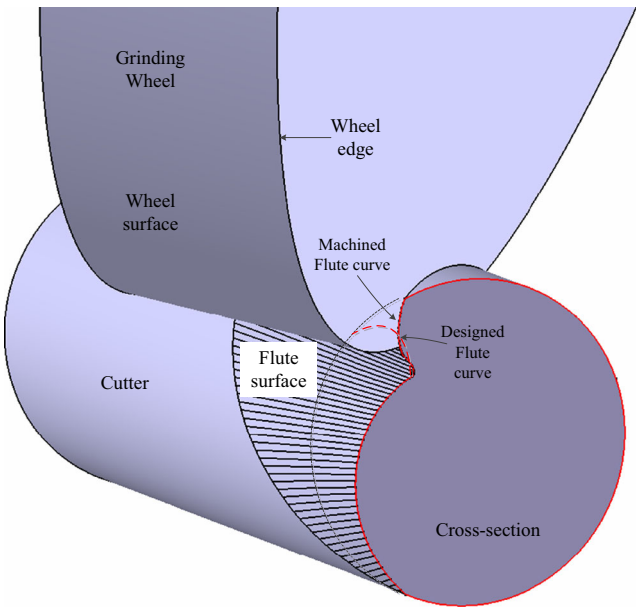

Fig. 6 Simulation for the interference in the flute-grinding processes

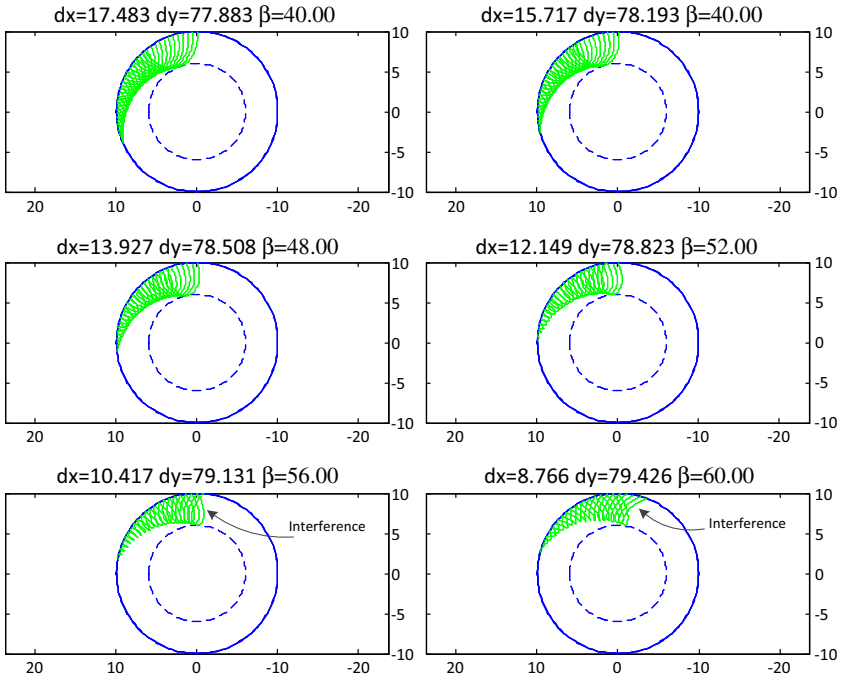

Fig. 7 Flute shape with various setting up parameters

cutter profile. The point P_S has been introduced in above section, and the point P_S'also satisfy the following geometrical condition: $|O_T P_S'|=r_T$. Recalling Eq. (10), the corresponding solution for point $P_S$and P_S' is denoted as θ_S^* and θ_{SS}^*. Golden search method is used to search the solutions for Eq. (10), and the searching range for θ is set as $\theta_S^* \in [0 \quad \theta_c^*]$ for point P_S and $\theta_{SS}^* \in [\theta_c^* \quad 2\pi]$ for point P_S'

where, θ_c^* is the parameter for point P_c and can be calculated by minimizing the distance from point $\boldsymbol{O_T}$ to the twist curve $P_S P_S'$, which will be explained in the following section.

Hereto, the solution for the corresponding points $P_S$and P_S' is denoted as the following:$\theta_S^* = \theta_S(dx \quad dy \quad \beta)$ and $\theta_{SS}^* = \theta_{SS}(dx \quad dy \quad \beta)$.

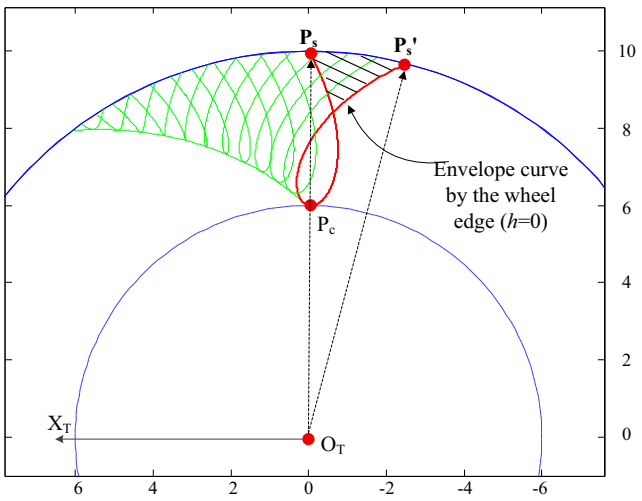

Fig. 8 Interference for flute profile in cross section

Substituting θ_S^* and θ_{SS}^* into Eq. (10), the point $P_S$and P_S' can be expressed as

$$P_S(\theta_S^*) = \begin{bmatrix} dx\cdot\cos t^* - dy\cdot\sin t - R\cdot\sin\theta_S^*\cdot\sin t + R\cdot\cos\beta\cdot\cos\theta_S^*\cdot\cos t^* \\ dx\cdot\sin t^* + dy\cdot\cos t + R\cdot\sin\theta_S^*\cdot\cos t + R\cdot\cos\beta\cdot\cos\theta_S^*\cdot\sin t^* \end{bmatrix} \quad (23)$$

$$P_S'(\theta_{SS}^*) = \begin{bmatrix} dx\cdot\cos t^* - dy\cdot\sin t - R\cdot\sin\theta_{SS}^*\cdot\sin t + R\cdot\cos\beta\cdot\cos\theta_{SS}^*\cdot\cos t^* \\ dx\cdot\sin t^* + dy\cdot\cos t + R\cdot\sin\theta_{SS}^*\cdot\cos t + R\cdot\cos\beta\cdot\cos\theta_{SS}^*\cdot\sin t^* \end{bmatrix} \quad (24)$$

In Fig. 8, the rake flute curve of segment $P_c P_S$ is intersected by the other part of the segment $P_c P_S'$. It can be explained that the flute profile generated by wheel edge $P_c P_S$ is ground by wheel edge $P_c P_S'$ in the segment succeeding grinding processes. In order to avoid the interference, the curve $P_c P_S'$ should not cross the curve $P_c P_S'$. From the geometrical point of view, it should satisfy the following condition:

$$\left(O_T P_S \times O_T P_S'\right)\cdot Z_T < 0 \quad (25)$$

where $O_T P_S'$ and $O_T P_S$ are the vectors shown in Fig. 8.

As shown in Fig. 9, the inequality for point P_s' and P_s can be applied to check interference. $(O_T P_s \times O_T P_s')\cdot Z_T=0$ is the critical condition for the interference. For the given wheel position$[dx \quad dy]$, the critical setup angle β^* can be calculated with the critical interference condition. And, the setup angle should satisfy the condition: $\beta<\beta^*$. Figure 9 shows an example for the avoidance of interference with the proposed condition:

1. Figure 9a is the normal condition for the enveloping flute with the condition: $(O_T P_s \times O_T P_s')\cdot Z_T<0$

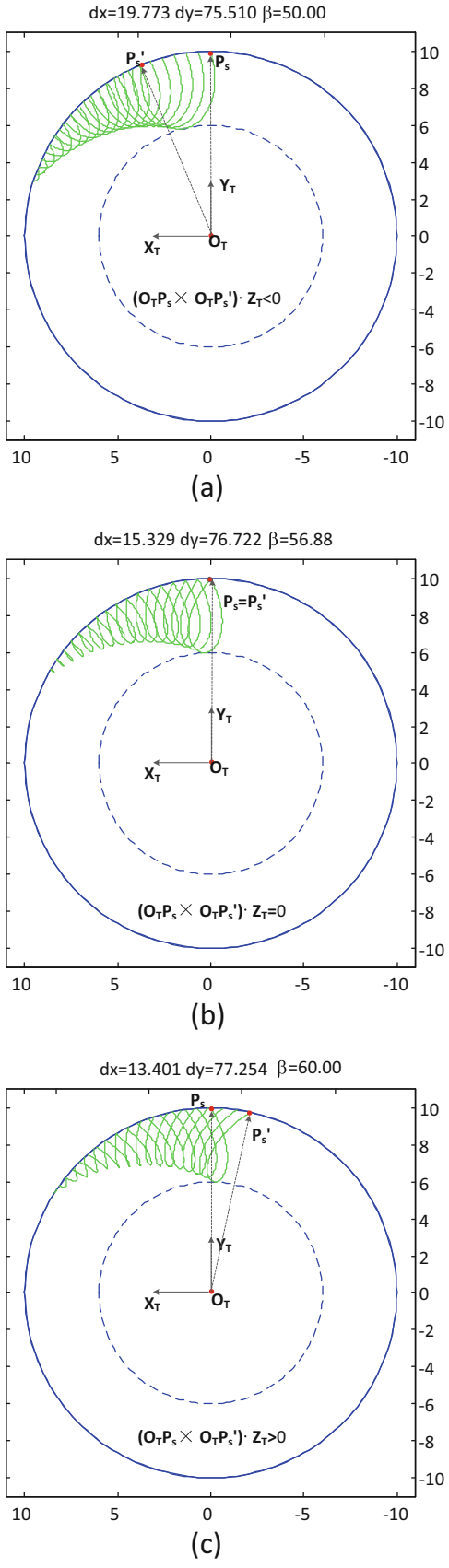

Fig. 9 Flute grinding with various condition: **a** non-interference, **b** critical condition, and **c** interference condition

2. Figure 9b is the critical condition for the enveloping flute with the condition: $(O_{\mathbf{T}}P_{\mathrm{s}} \times O_{\mathbf{T}}P_{\mathrm{s}}^{'}) \cdot Z_{\mathbf{T}} = 0$
3. Figure 9c is the interference condition for the enveloping flute with the condition: $(O_{\mathbf{T}}P_{\mathrm{s}} \times O_{\mathbf{T}}P_{\mathrm{s}}^{'}) \cdot Z_{\mathbf{T}} > 0$

3.3 Flute profile generated by wheel edge exclusively

As aforementioned, in the flute-grinding processes, the flute surface is ground via two parts of the grinding wheel: one section grinding by the wheel edges and the other section is generated by envelope of the wheel surface. However, if the wheel is mounted with a larger setup angle β and the wheel location with a larger dx than dy, the flute curve will be generated by the wheel edge exclusively. As shown in Fig. 10, the red line is the flute profile whose final shape is determined by the wheel edge exclusively. Since wheel edge is the weak part of the grinding wheel, it will accelerate the wear of the grind wheel or even the breakage. Besides, the flute profile generated by the wheel edge exclusively with a larger negative value will result in great cutting forces in the milling processes. Therefore, such kind of flute profile is not acceptable in engineering.

Similarly with the above section, another geometrical condition for the wheel setting parameters is introduced to avoid the wheel edge grinding exclusively. As described in Fig. 11, the flute curve was exclusively generated by the wheel edge and the envelope part exceeds the cutter profile. $\boldsymbol{P_o}$ is the start point of the envelope flute curve, and it is also the connect point between the wheel edge and wheel surface while grinding the flute. Setting h=0 for Eq. (15), for the given wheel setting parameters, we can get the solution for $\theta_{\mathrm{o}}^{*} = \theta_{\mathrm{o}}(dx \quad dy \quad \beta)$ which is a parameter for point $\boldsymbol{P_o}$.

Recalling Eq. (10), the expressions of point $\boldsymbol{P_o}$ can be obtained:

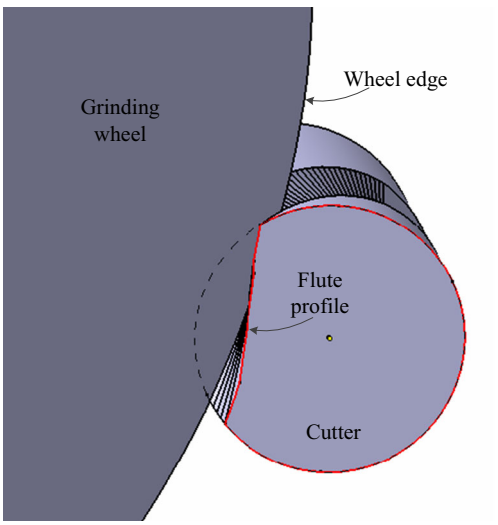

Fig. 10 Flute profile ground by wheel edge exclusively

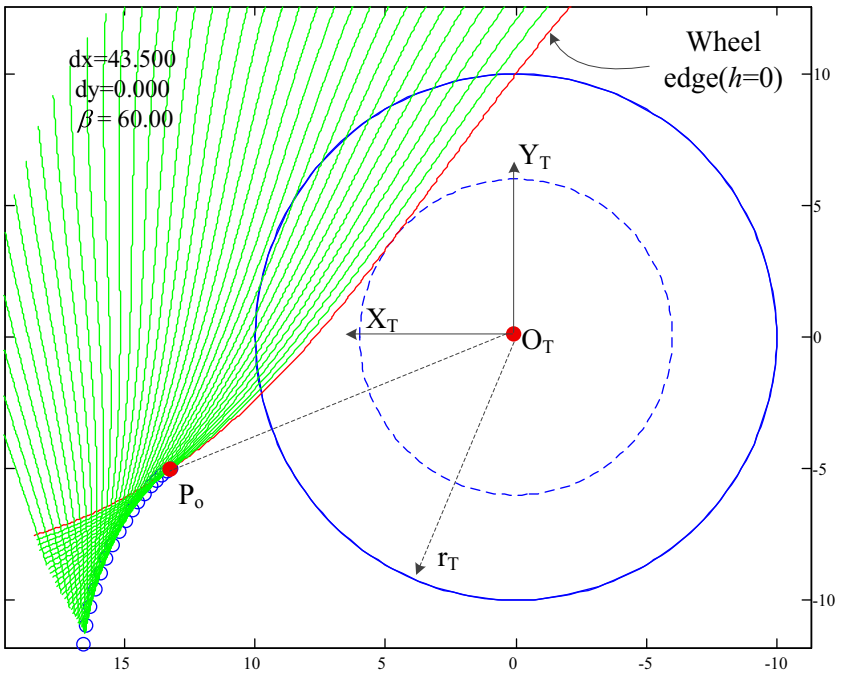

Fig. 11 The flute curve generated by the wheel edge (h=0)

$$P_o = \begin{bmatrix} dx\cdot\cos t - dy\cdot\sin t - R\cdot\sin\theta_o^*\cdot\sin t + R\cdot\cos\beta\cdot\cos\theta_o^*\cdot\cos t \\ dx\cdot\sin t + dy\cdot\cos t + R\cdot\sin\theta_o^*\cdot\cos t + R\cdot\cos\beta\cdot\cos\theta_o^*\cdot\sin t \end{bmatrix}$$

Figure 12 shows a generalized flute profile with the wheel edge grinding and wheel surface envelope grinding. From geometrical point of view, point P_o should be inside of the cutter profile, while keeping outside of the core area to avoid interference of the core radius, that is $r_c<|O_TP_o|<r_T$. From above analysis, the point $\boldsymbol{P_o}$ can be considering as an implicit function of wheel setting parameters. Thus, the inequality for $\boldsymbol{P_o}$ can be applied to check the wheel setting parameters to avoid the wheel edge exclusively grinding.

An example is given with two sets of wheel setting to demonstrate the application of the constraints for point $\boldsymbol{P_o}$.

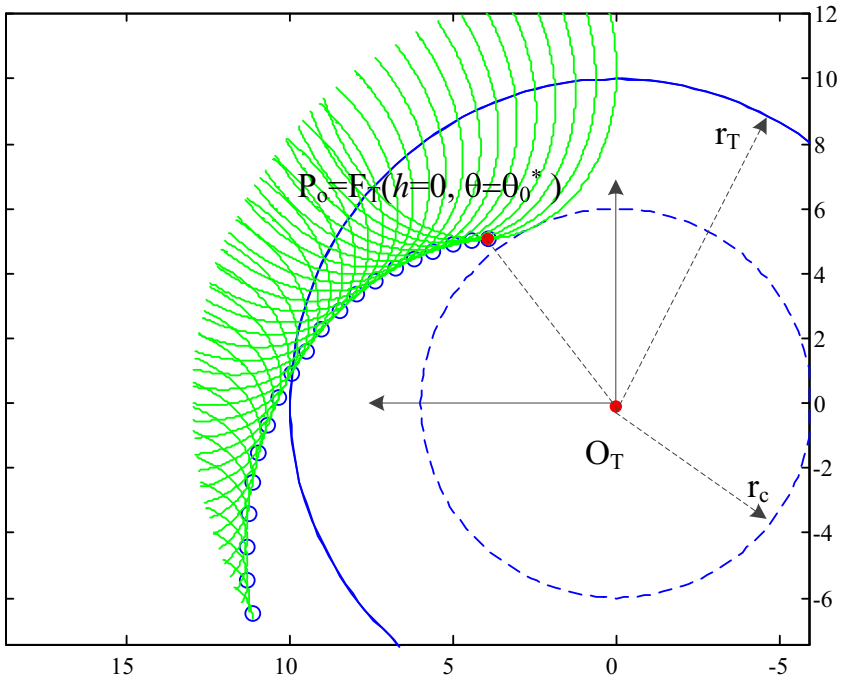

Fig. 12 Geometrical constraint for envelope point P_o

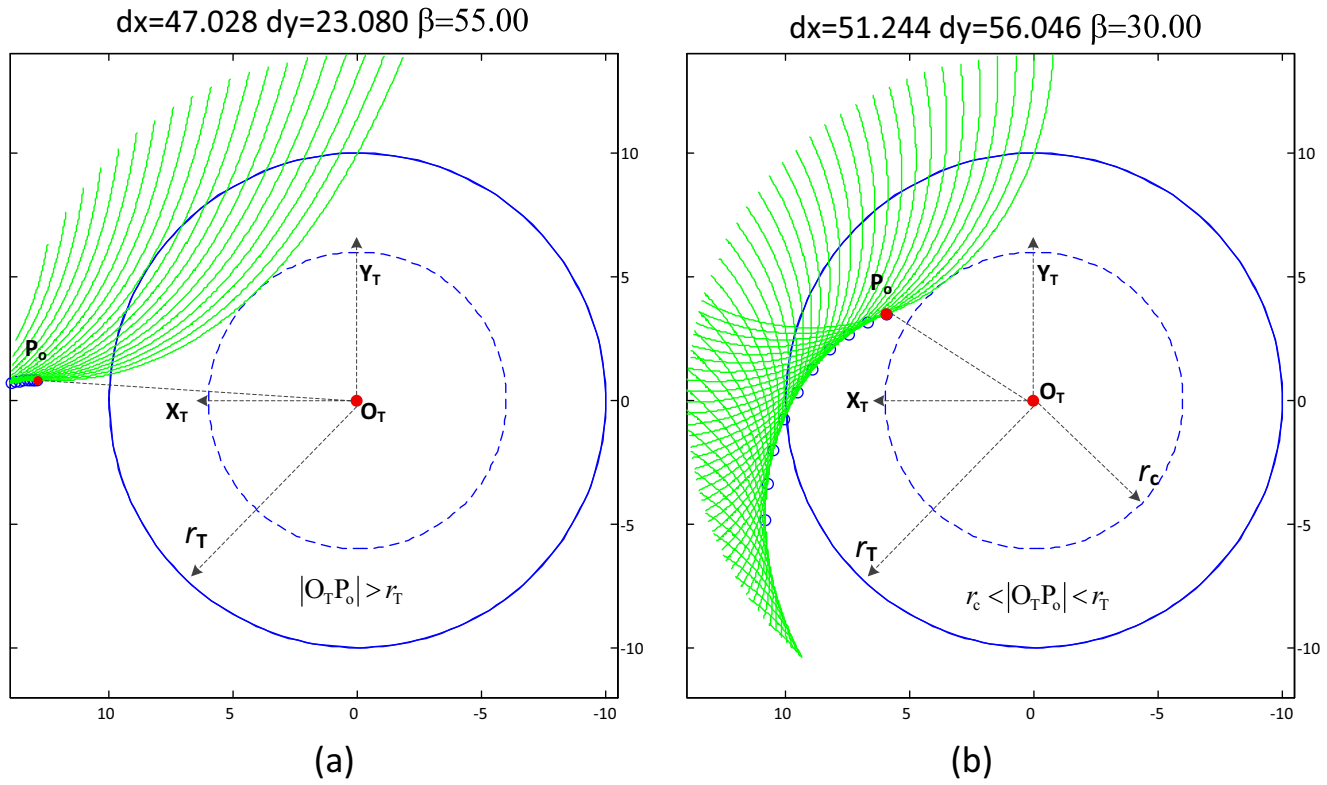

Fig. 13 Flute profile simulation: **a** wheel edge exclusively grinding and **b** flute generalized flute

Figure 13b shows a generalized flute profile with the constraint: $r_c<|O_TP_o|<r_T$, while the flute in Fig. 13a is ground by the wheel edge exclusively with the constraint: $|O_TP_o|>r_T$.

4 Determination of the wheel's position and orientation

4.1 Modeling the optimization problem

In the flute-grinding processes, we always hope that the machined flute parameters approximates to the designed flute parameters as close as possible. Based on the proposed five-axis CNC grinding model, the machined flute parameters can be regarded as a function in terms of the wheel's position and orientation. Mathematically, the problem now is restated as: given the designed flute parameters to calculate the wheel's position and orientation expressed in Eq. (26)

$$\begin{cases} f_{rake}(dx \quad dy \quad \beta) = \gamma_0 \\ f_{flute}(dx \quad dy \quad \beta) = \phi_0 \\ f_{core}(dx \quad dy \quad \beta) = r_{c0} \end{cases} \tag{26}$$

where $\{\gamma_0 \quad \phi_0 \quad r_{c0}\}$ is the designed flute parameters and $\{dx \quad dy \quad \beta\}$ is the unknown wheel position and orientation which are required to be calculated.

In this research, the solutions for the equations are transferred into an optimization problem through the two steps:

Step I. Normalize the flute parameters:

Physically, the flute parameters are measured with different units and scale. In order to evaluate the calculated results in the same level, a normalization processes is used in this research shown in Eq. (27). $f_{norm}(x)$ is a normalized function, which can be used to define the flute parameters in the unit level so as to eliminate the effect of units and scales mentioned above.

$$f_{norm}(x) = \frac{x - x_{\min}}{x_{\max} - x_{\min}} \tag{27}$$

We define the minima ($x_{\min}$) and maxima ($x_{\max}$) for the flute parameters based on the engineering practice: $r_c \in [0, \quad r_T]$, $\gamma \in [-20, \quad 30]$ and $\phi \in [0, \quad 180]$.

Step II. Calculate the difference between the normalized designed flute parameters and machined flute parameters:

After normalizing the flute parameters,

the solution for Eq. (26) can be transferred into solving the equivalent equation in Eq. (28).

$$\sqrt{\begin{array}{l}(f_{norm}(f_{rake}(\,dx \quad dy \quad \beta))-f_{norm}(\gamma_0))^2+\left(f_{norm}\left(f_{flute}(\,dx \quad dy \quad \beta)\right)-f_{norm}(\phi_0)\right)^2\\ +(f_{norm}(f_{core}(\,dx \quad dy \quad \beta))-f_{norm}(r_{c0}))^2\end{array}}=0 \tag{28}$$

If the solution exists, it can be reformulated as a minimizing problem with the objective function in Eq. (29):

$$min\left(\sqrt{\begin{array}{l}(f_{norm}(f_{rake}(\,dx \quad dy \quad \beta))-f_{norm}(\gamma_0))^2+\left(f_{norm}\left(f_{flute}(\,dx \quad dy \quad \beta)\right)-f_{norm}(\phi_0)\right)^2\\ +(f_{norm}(f_{core}(\,dx \quad dy \quad \beta))-f_{norm}(r_{c0}))^2\end{array}}\right) \tag{29}$$

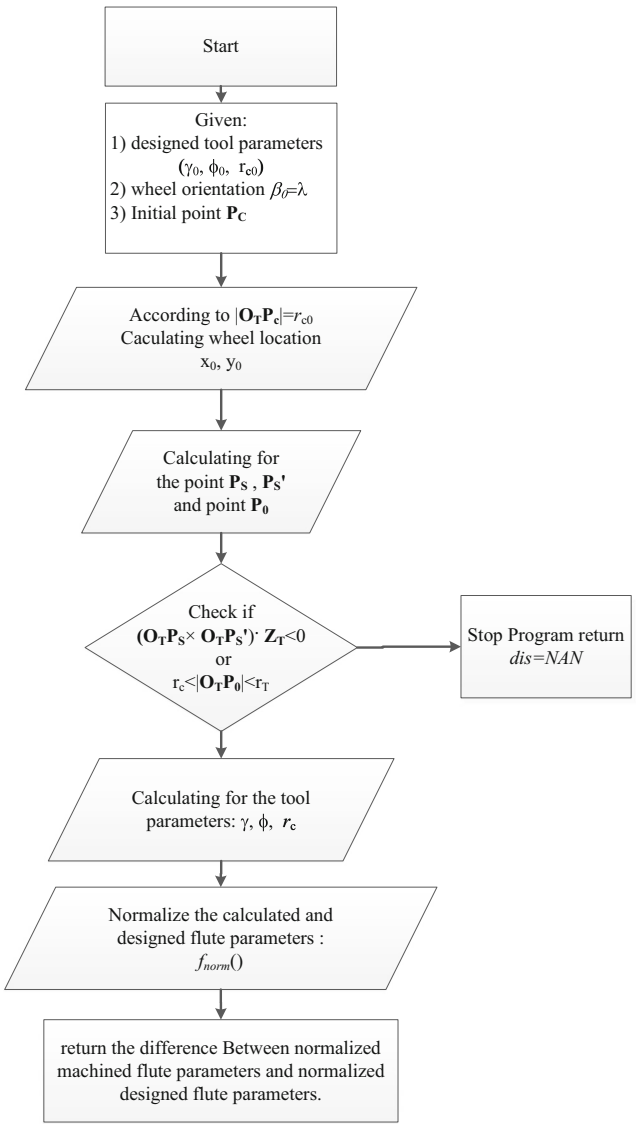

Fig. 14 Flowchart of optimization model for flute grinding

And also, in order to avoid the interference mentioned above, the possible solution of Eq. (29) should satisfy the following constraint conditions:

$$\begin{cases}P_c|_{(\,dx \quad dy \quad \beta)}\in S\\ \left(O_TP_S\times O_TP_S'\right)\cdot Z_T\big|_{(\,dx \quad dy \quad \beta)}<0\\ r_c<|O_TP_o|_{(\,dx \quad dy \quad \beta)}<r_T\end{cases} \tag{30}$$

It is obvious that the solution for Eq. (28) is equivalent to the minimized result of Eq. (29) if the objective function could be infinitesimal. A Matlab program was developed to represent Eq. (29) with the constraint conditions in Eq. (30). The optimization model is summarized in the following flowchart shown in Fig. 14: First, an initial point $\boldsymbol{P_c}$ in terms of θ_c and wheel orientation β are given, which can be used to calculate the wheel's location $[\,dx \quad dy\,]$ through the contact constraint. Afterwards, the inequality constraints in Eq. (30) are used to check the validity of the initial value; if invalid, a NaN value will be returned. Then, the flute parameters can be calculated based on the provided wheel's position and orientation through the proposed envelope theory within cross section. After normalizing the flute parameters, the value of Eq. (30)

Table 1 Parameters for flute-grinding process

Parameters for flute grinding		Value
Tool parameters	Tool radius $\boldsymbol{r_T}$ (mm)	10
	Core radius $\boldsymbol{r_{c0}}$ (mm)	7
	Rake angle $\boldsymbol{\gamma_0}$ (°)	8
	Flute angle $\boldsymbol{\phi_0}$ (°)	75
	Helix angle $\boldsymbol{\lambda}$ (°)	45
Wheel parameters	Wheel width $\boldsymbol{H}$ (mm)	30
	Wheel radius $\boldsymbol{R}$ (mm)	75

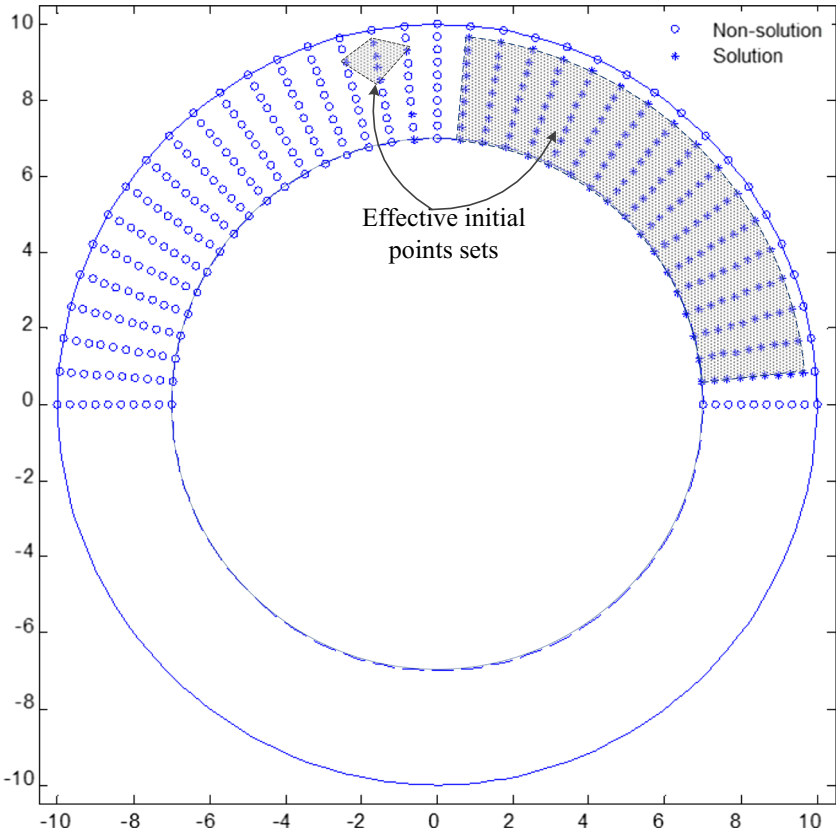

Fig. 15 Initial points for the optimization model

is easily calculated so as to evaluate the difference. It is noted that the optimization model is programmed with a series of complicated numerical calculation which brings in the fluctuation of objective function while the solution approaches to high accuracy. *Fminsearch* is a common search function in Matlab toolbox used for nonlinear optimization technique based on the "*Nelder-Mead simplex direct search*" algorithm. This method often handle discontinuity problem without providing any derivative information. Hereto, *fminsearch* is used to solve the optimization model.

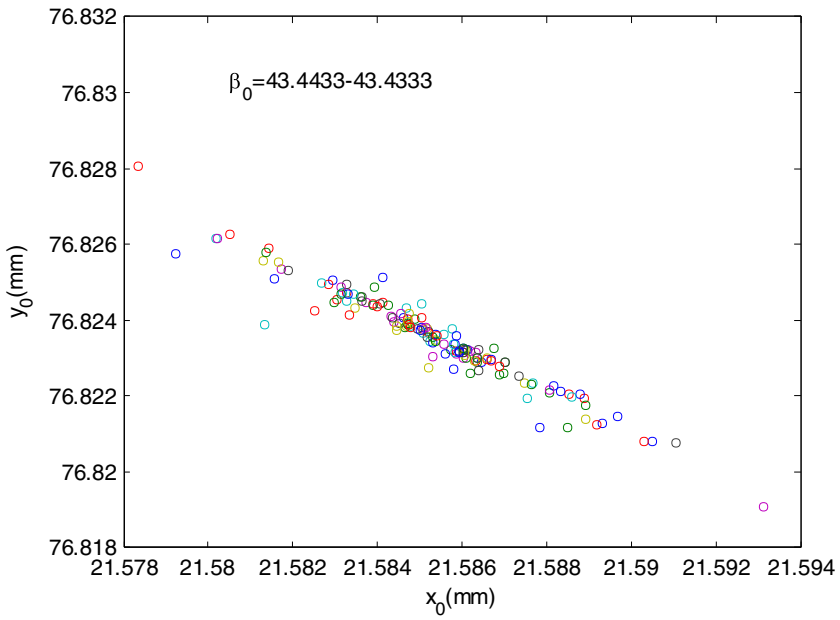

Fig. 16 Solution for the wheel position and orientation

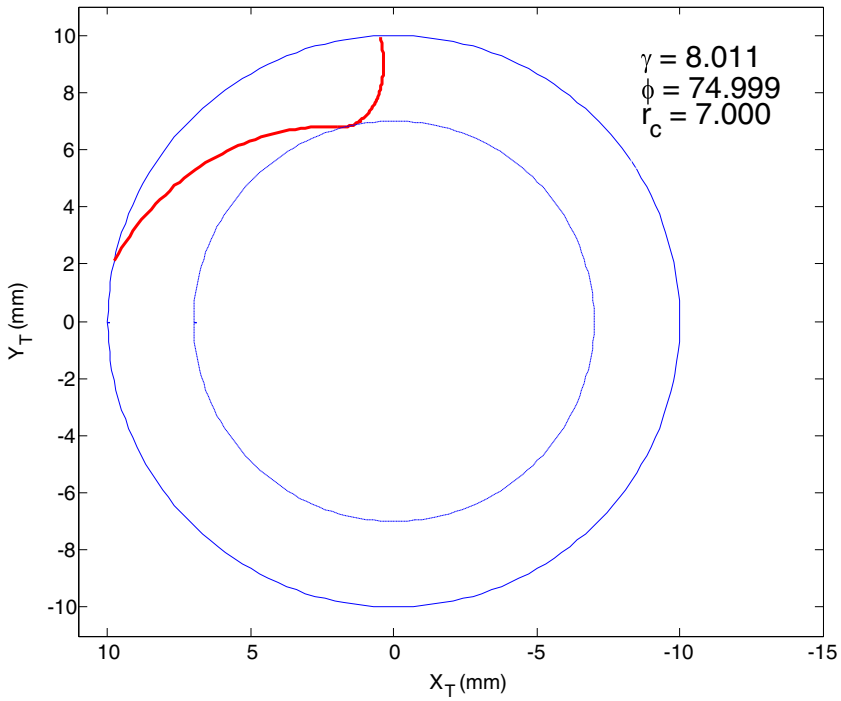

Fig. 17 The machined flute parameters and flute profile

4.2 Verification

In the above two steps, the five-axis flute-grinding processes was converted to an equivalent optimization model. An example was given in this research. The designed flute parameters and grinding wheel specification are provided in Table 1. Based on the engineering experience, the initial value for orientation parameter β was generally setting 45° the same value as helix angle λ. And also, a group of initial points for the optimization model were investigated in the contacting area ($P_c \in S$) to test the validity and efficiency of solution shown in Fig. 15. The optimized results with various initial points were described with different markers: The circle marks represent that the optimized results can satisfy the solution with acceptable tolerance (1e-4), while the star makers mean not. It was observed that the solutions existed while the initial points were set in the first quadrant of contact area $\boldsymbol{S}$ which was shaded as effective initial points set in Figs. 15 and 16 that showed that the solutions with various initial points converge within a tolerance area, which means that the objective function in this example was convex with only one solution existing in the feasible area. In this example, suppose the grinding speed is 1500 RPM, the feed rate is 10 mm/s, and rotation speed is 1 rad/s calculated by Eq. (8), the solution of wheel's position and orientation were obtained using the developed Matlab program with the values 21.585, 76.823, and 43.437. The machined flute parameters and generated flute profile were calculated and plotted in Fig. 17 which closely approximated to the designed flute parameters in Table 1. Besides, the elapse time of running the optimization program was also obtained with 0.293 s 51 iterations which were quite efficient compared with the Boolean operation method [11, 12] which took around 5.3 min for only one iteration of grinding simulation in this case.

To demonstrate the validity and versatility of the proposed method, we designed several various flute shapes with a large range of flute parameters and tool parameters in Table 2. The grinding speed and feed rate in this grinding process was

Table 2 Verification of optimized model (length unit: mm, angle unit: °)

No.	Tool parameters ($\boldsymbol{\lambda}$, $\boldsymbol{r_T}$)	Designed flute parameters ($\boldsymbol{\gamma_0}$, $\boldsymbol{\phi_0}$, $\boldsymbol{r_{c0}}$)	Solution of wheel's pos. and orient. (dx, dy, β)	Machined flute parameters ($\boldsymbol{f_{rake}}$, $\boldsymbol{f_{flute}}$, $\boldsymbol{f_{core}}$)
1	45, 10	(8, 75, 6)	(29.984, 69.913, 44.859)	(7.994, 74.999, 6.000)
2	45, 10	(15, 80, 7)	(16.978, 78.629, 45.598)	(15.001, 8.001, 7.000)
3	45, 10	(15, 160, 7)	(4.806, 81.760, 42.177)	(15.002, 159.996, 7.000)
4	38, 5	(10, 80, 3)	(5.875, 78.476, 51.490)	(10.008 79.992, 4.000)
5	35, 5	(5, 170, 3.5)	(2.743, 78.406, 45.630)	(5.002 170.001, 3.500)
6	38, 5	(−5, 50, 4)	(6.485, 78.125, 58.729)	(−5.000, 50.001, 4.000)

suggested as 1500 RMP and 10 m/s, respectively. The wheel position and orientation were determined with the proposed method listed (Table 2). For illustrative purpose, the flute grinding was simulated in the CAD/CAM software CATIA via Boolean operation and the solid flute model was obtained in Fig. 18. To verify the flute parameters, the rake angle, flute angle, and core radius were measured with CAITA "*measure*" function illustrated in Fig. 18, which also showed an accurate agreement with the designed flute parameters.

Overall, with the above verification and simulation, the flute parameters can be accurately and efficiently guaranteed with the proposed method through determination of wheel's position and orientation in the CNC grinding processes. The results showed that the accuracy of machined flute parameters could achieve 1e-3 mm and 1e-2°, which satisfied the machining tolerance. Although, this method mainly focused on the flute-grinding processes, it provides a general model and solution for research on how to determine the wheel position and orientation for grinding operations, which could be extended to grind more complex designed surface in the future study. However, it is also noted that implementation of this method in practice still need more work to be considered, such as generating Gcode for the CNC grinding machine with the post-processing, planning of grinding speed and feed rate of the grinding wheel, strategy of online measurement for the machined part, and dynamic of CNC grinding machine.

5 Conclusions

In this paper, a novel approach for five-axis CNC flute grinding model was developed to machine the designed flute parameters. The machined flute profile and flute parameters were deduced through envelope of the grinding wheel in the

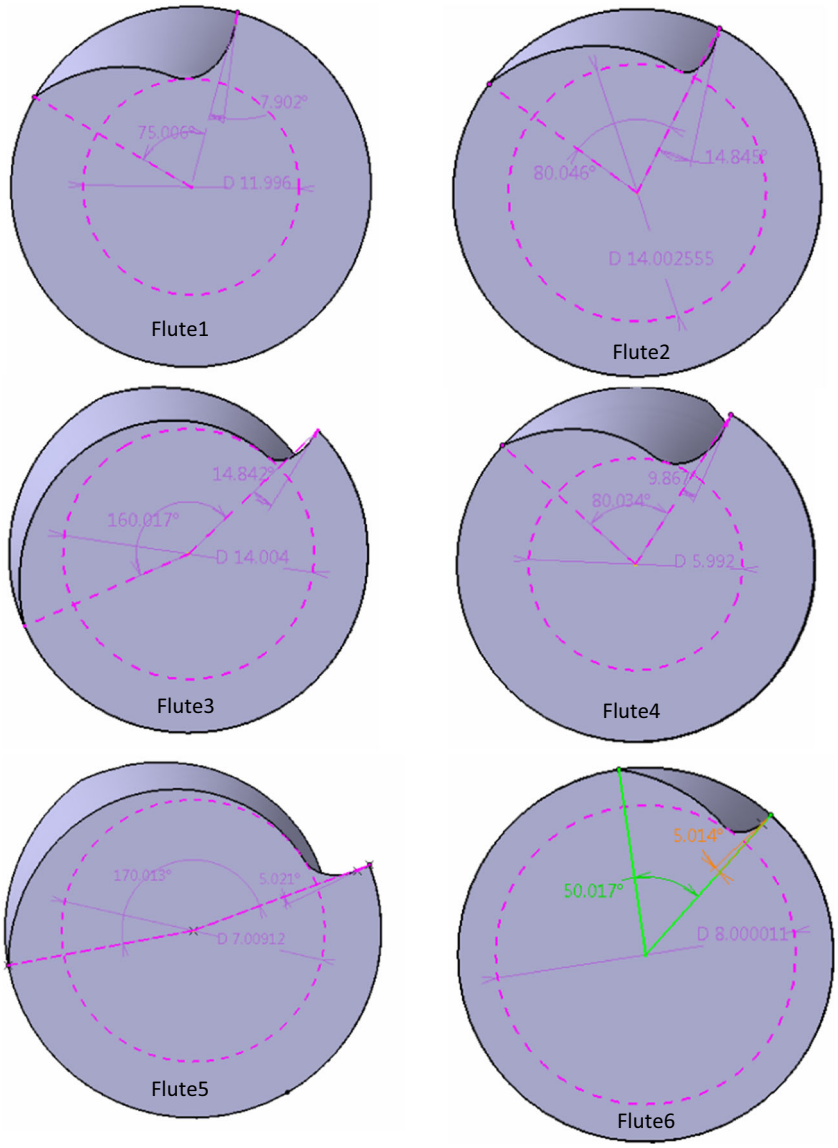

Fig. 18 The solid flute model generated by CATIA

cross section. On the basis of kinematics of five-axis CNC grinding algorithm, the geometrical constraints to avoid interference and abnormal flute profile were first developed in this work. The wheel's position and orientation were determined by an optimization model through minimizing the difference between machined flute parameters and designed requirements. The major contribution of this work was to develop the constraint optimization model for the five-axis flute-grinding processes. It was noted that, comparing with inverse method, the presented method was to grind the designed flute parameters with the standard grinding wheel rather than modifying the grinding wheel shape, which could facilitate the fluting operations. The simulation results showed that this approach could achieve a high accuracy and efficiency than the Boolean operation. Besides, controlling the grinding wheel to guarantee the designed parameters is a common problem in CNC grinding processes of end mills; thus, this method could be extended to other grinding operations, such as grinding relief surface.

Acknowledgments This work was partially supported by the Fundamental Research Funds of Shandong University (No. 2015HW020) and the National Natural Science Foundation of China (No. 51275277).

References

1. Wang LM, Chen ZC (2014) A new CAD/CAM/CAE integration approach to predicting tool deflection of end mills. Int J Adv Manuf Technol 72(9-12):1677–1686
2. Yan L, Jiang F (2013) A practical optimization design of helical geometry drill point and its grinding process. Int J Adv Manuf Technol 64(9-12):1387–1394
3. Kaldor S, Rafael AM, Messinger D (1988) On the CAD of profiles for cutters and helical flutes—geometrical aspects. CIRP Ann Manuf Technol 37(1):53–56
4. Ehmann KF, DeVries MF (1990) Grinding wheel profile definition for the manufacture of drill flutes. CIRP Ann Manuf Technol 39(1): 153–156
5. Kang SK, Ehmann KF, Lin C (1996) A CAD approach to helical groove machining. Part 1: mathematical model and model solution. Int J Mach Tools Manuf 36(1):141–153
6. Kang SK, Ehmann KF, Lin C (1997) A CAD approach to helical groove machining. Part 2: numerical evaluation and sensitivity analysis. Int J Mach Tools Manuf 37(1):101–117
7. Kang DC, Armarego EJA (2003) Computer-aided geometrical analysis of the fluting operation for twist drill design and production I. Forward analysis and generated flute profile. Mach Sci Technol 7(2):221–248
8. Kang DC, Armarego EJA (2003) Computer-aided geometrical analysis of the fluting operation for twist drill design and production. II. Backward analysis, wheel profile and simulation studies. Mach Sci Technol 7(2):249–266
9. Hsieh J (2009) Mathematical modeling of a complex helical drill point. ASME J Manuf Sci Eng 131(6):061006
10. Zhang W, Wang X, He F, Xiong D (2006) A practical method of modelling and simulation for drill fluting. Int J Mach Tools Manuf 46(6):667–672
11. Kim JH, Park JW, Ko TJ (2008) End mill design and machining via cutting simulation. CAD 40(3):324–333
12. Li G, Sun J, Li JF (2014) Process modeling of end mill groove machining based on Boolean method. Int J Adv Manuf Technol 75:959–966
13. Ren B, Tang Y, Chen C (2001) The general geometrical models of the design and 2-axis NC machining of a helical end-mill with constant pitch. J Mater Process Technol 115(3):265–270
14. Lin SW, Lai HY (2001) A mathematical model for manufacturing ball-end cutters using a two-axis NC machine. Int J Adv Manuf Technol 17(12):881–888
15. Chen J, Lee B, Chen C (2008) Planning and analysis of grinding processes for end mills of cemented tungsten carbide. J Mater Process Technol 201:618–622
16. Feng X, Hongzan B (2003) CNC rake grinding for a taper ball-end mill with a torus-shaped grinding wheel. Int J Adv Manuf Technol 21(8):549–555
17. Hsieh J, Tsai Y (2006) Geometric modeling and grinder design for toroid-cone shaped cutters. Int J Adv Manuf Technol 29(9-10):912–921
18. Chen F, Bin H (2009) A novel CNC grinding method for the rake face of a taper ball-end mill with a CBN spherical grinding wheel. Int J Adv Manuf Technol 41(9-10):846–857
19. Pham TT, Ko SL (2010) A manufacturing model of an end mill using a five-axis CNC grinding machine. Int J Adv Manuf Technol 48(5-8):461–472